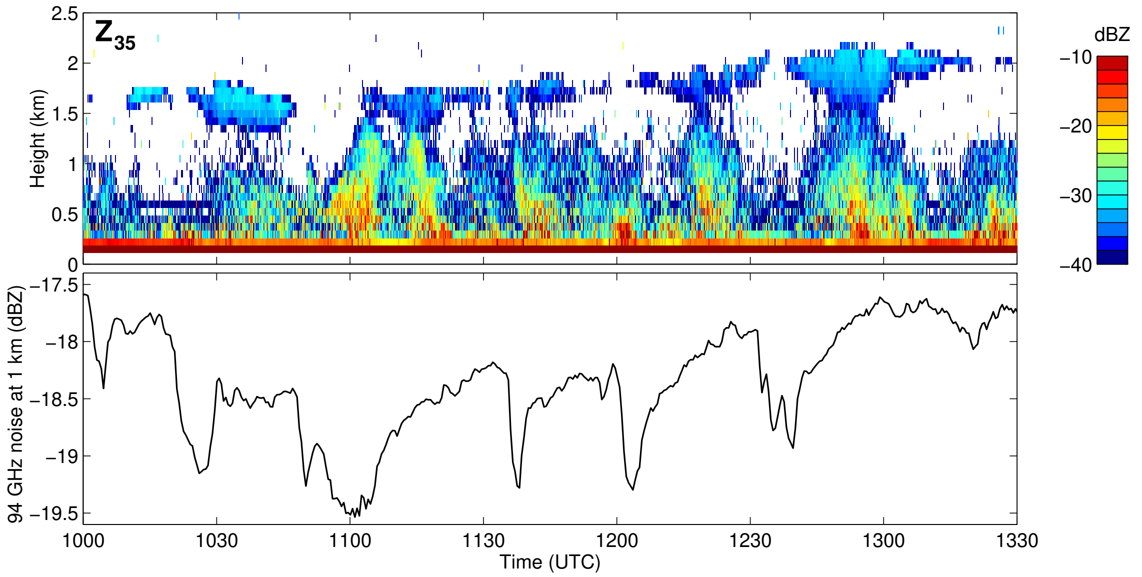

Figure 2.2: Time series of reflectivity factor through low cloud and insects at 35 GHz, and the corresponding noise-equivalent reflectivity at 1 km measured by the 94 GHz radar (using the cloud-free gates in the stratosphere). The data were taken on 23 June 1996.

2.2.4 Noise subtraction

An important way to improve the sensitivity of the radar is to subtract an estimate of the noise $\hat{N}$ from the measured average power $\bar{P}$, where 'noise' is taken to be the sum of receiver noise and thermal emission by the atmosphere, as they are generally indistinguishable. This enables the minimum detectable signal to be reduced by at least an order of magnitude below the noise level. Often rain radars simply reject the data that fall below a particular threshold, which is far too crude a procedure if quantitative use is to be made of observations at low reflectivity. The noise component manifests itself as a constant power with range, so in practice $\bar{P}$ in the cloud-free stratosphere provides an accurate measure of $\hat{N}$. In this section we determine the effect of noise subtraction on the accuracy of the final Z measurement, as a function of signal-to-noise ratio SNR $= \bar{S}/\bar{N}$.

One should be aware that $\hat{N}$ exhibits significant variability from one minute to the next, so should be calculated separately for every ray (but not every pulse); this is illustrated in Fig. 2.2 which shows $\hat{N}$ at 94 GHz as a function of time, together with the 35 GHz reflectivity factor in the lowest 2 km of the atmosphere. It can be seen that the thermal emission varies by as much as 2 dB as low clouds pass overhead, because the radar is essentially acting as a microwave radiometer. The same behaviour was observed at 35 GHz, but the amplitude of the variation was less. Note that the insects beneath the cloud have no discernible radiative effect.

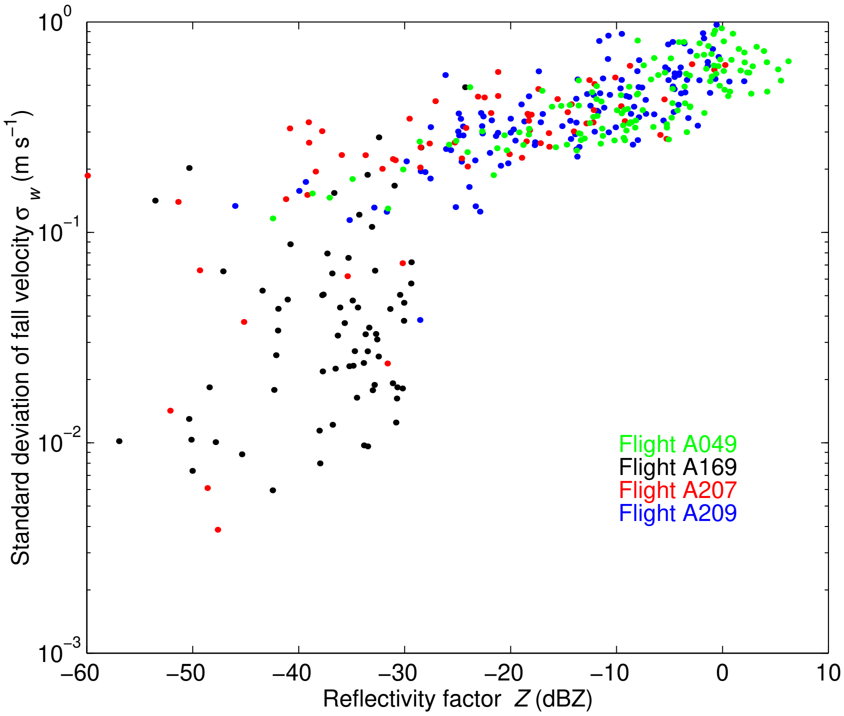

Figure 3.2: The standard deviation of still-air Doppler spectra from four flights during ASTEX. Each point represents a 100 second average, and in total there are 21 hours of data.

-30 dBZ (and many below) contain drizzle and therefore have a value for σ_w of greater than 20 cm s^{-1}. Incidentally, this is at odds with the assertion of Frisch et al. (1995) that all warm stratiform clouds with a reflectivity less than -17 dBZ are drizzle-free. Any turbulence in the cloud will increase σ_w above the value due to differential fall speeds alone, and hence reduce the time to independence and increase the accuracy of retrieved LWC.

Considering the typical values $\sigma_w = 25$ cm s^{-1}, $\delta = 75$ m, and T =10°C, we find that to retrieve LWC to an accuracy of 0.05 g m^{-3} with no vertical averaging requires a dwell time of nearly 6 minutes. This value of σ_w implies that only 200 pulses are independent per second at 35 GHz, and only 550 at 94 GHz. For a resolution of 150 m, the required dwell time is reduced to 44 seconds, and a resolution of 300 m requires only a 5.5 second dwell. It is the clear that there is much to be gained from spatial averaging.

The effect of errors in temperature

Naturally there will be errors in the temperature profile over the radar site as taken from either a model or radiosonde ascents, and it is important to know how these would affect retrievals due to the temperature dependence of the attenuation coefficients and the dielectric constant. We can assume that the relative humidity will be very close to 100% wherever cloud is detected, so therefore a large

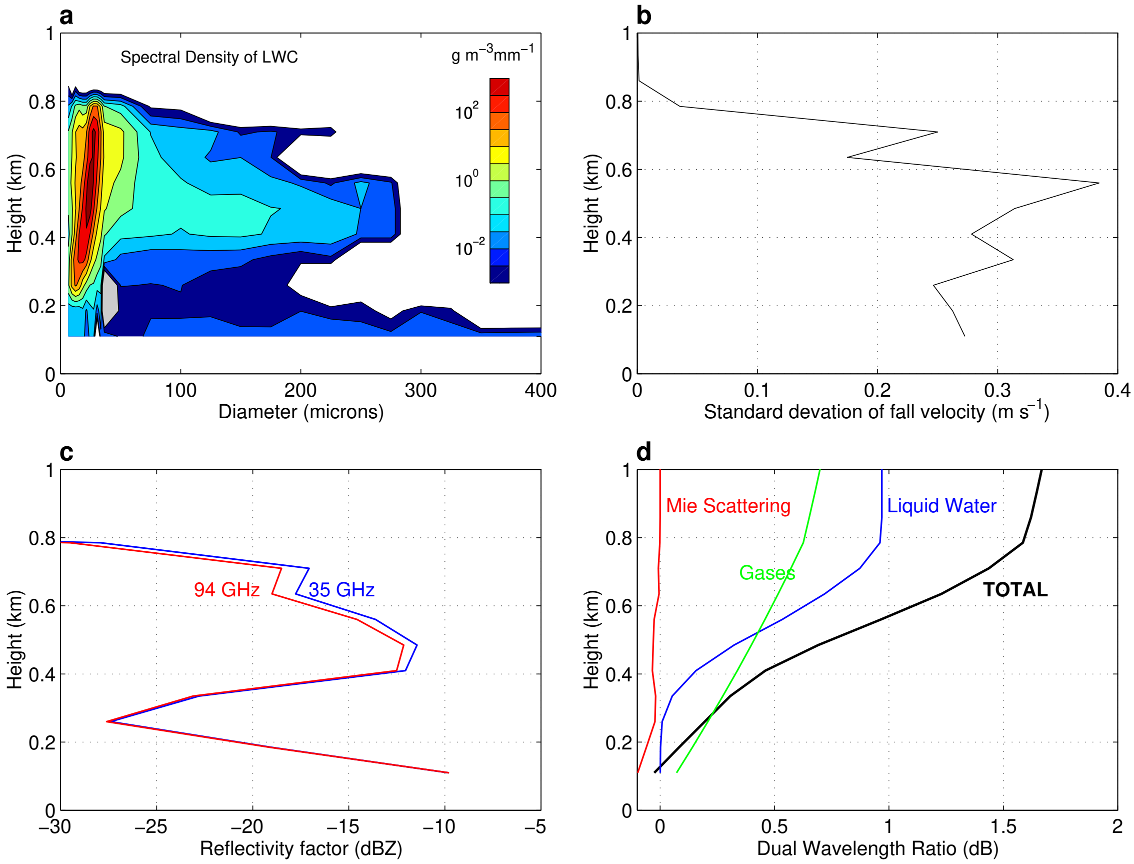

Figure 3.4: Aircraft profile through stratocumulus during flight A209 (12 June 1992) of: **(a)** Spectral density of liquid water content versus diameter; **(b)** Standard deviation of the still-air Doppler spectrum σ_w; **(c)** Simulated reflectivity at 35 and 94 GHz, taking account of Mie scattering and attenuation due to both liquid water and atmospheric gases (using a suitable profile of temperature and humidity with a surface temperature of around 10°C); **(d)** Simulated total DWR, and the individual components due to Mie scattering, attenuation by liquid water and attenuation by atmospheric gases.

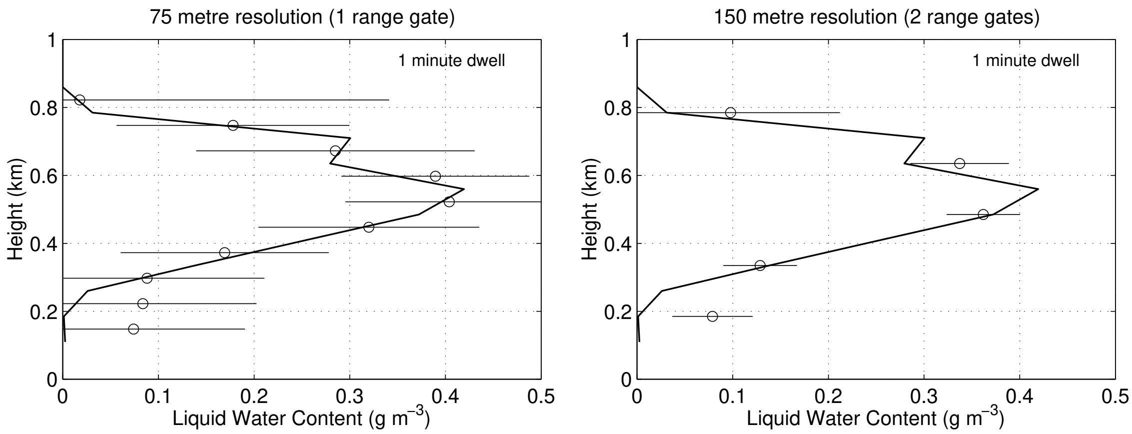

Figure 3.5: Profile of LWC from the same case as in Fig. 3.4 (solid line), with the error bars indicating the corresponding simulated measurements by a ground-based dual-wavelength radar for a one-minute dwell and both no averaging (left plot) and 2-gate averaging (right plot).

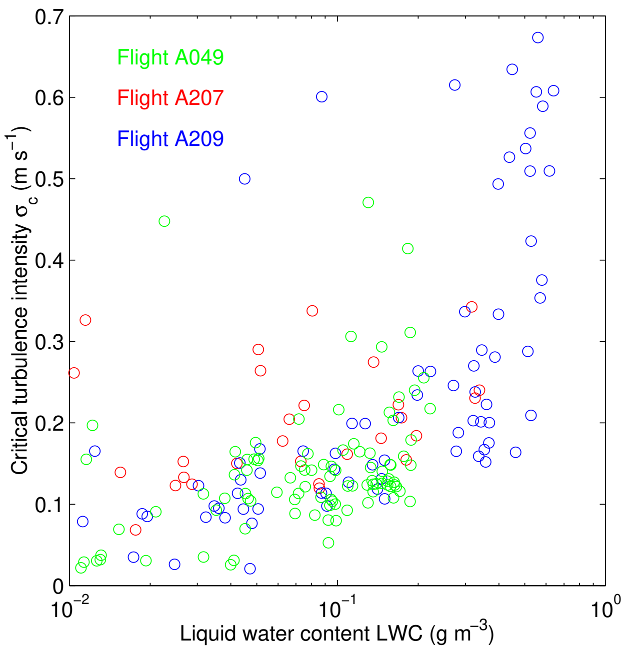

Figure 3.9: The critical air vertical-velocity standard deviation at which the cloud component loses its identity, as a function of LWC.

the cloud component of the spectrum in still-air can be represented by a delta function at $w = 0$, and that the drizzle component can be approximated by a Gaussian distribution with the same mean and standard deviation. This is a fairly straightforward mathematical task since both the delta function and the Gaussian distribution can be convolved analytically with Gaussian turbulence. This method gives values for σ_c of 30 and 9 cm s^{-1} for the spectra in Figs. 3.7 and 3.8 respectively, which compares well with the exact calculations of the effect of turbulence and indicates that this approach is robust.

Figure 3.9 shows σ_c as a function of LWC. It can be seen that when LWC is greater than 0.1 g m^{-3}, all but one of the samples have a value of σ_c greater than 10 cm s^{-1}. For smaller values of LWC, σ_c can be less than 5 cm s^{-1}, corresponding to clouds for which the reflectivity of the drizzle drops is at least 40 dB larger than that of the cloud droplets. In this analysis we have rejected all observations for which the reflectivity of the cloud droplets Z_c is more than twice the reflectivity of the drizzle drops, since for these it is unimportant whether the two components can be separated. Of the clouds in these three flights with an LWC of greater than 0.01 g m^{-3}, in only 5% was this found to be the case.

These values should be compared with the typical values of σ_a that are found in stratocumulus. Gossard et al. (1997) showed an example of a real stratocumulus Doppler spectrum measured with a 35 GHz radar, for which they calculated that σ_a =16 cm s^{-1}. This is larger than the critical

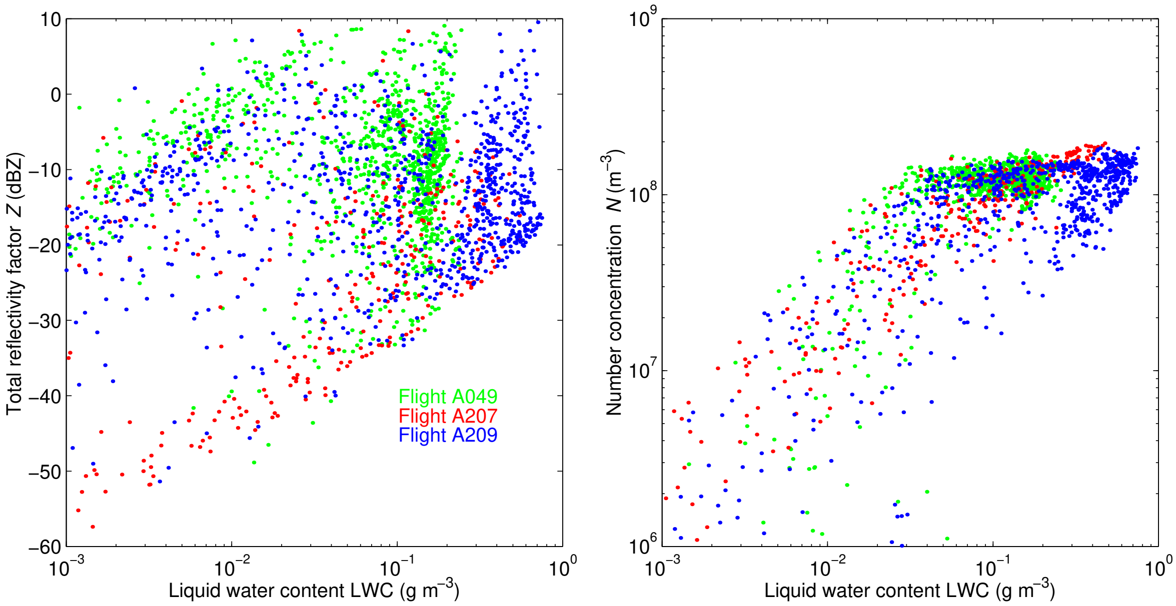

Figure 3.12: Scatterplots of total reflectivity factor and total number concentration, versus LWC, for three ASTEX flights containing drizzle.

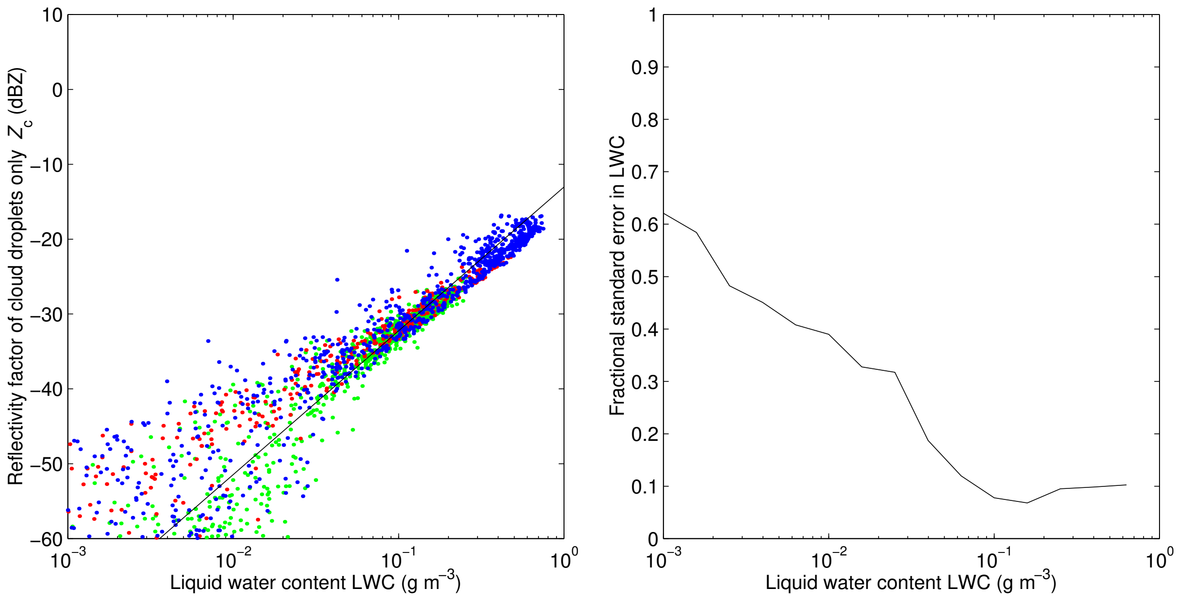

Figure 3.13: Scatterplot of the reflectivity factor of the cloud droplets alone versus LWC, and the corresponding fractional error in LWC as measured using (3.26).

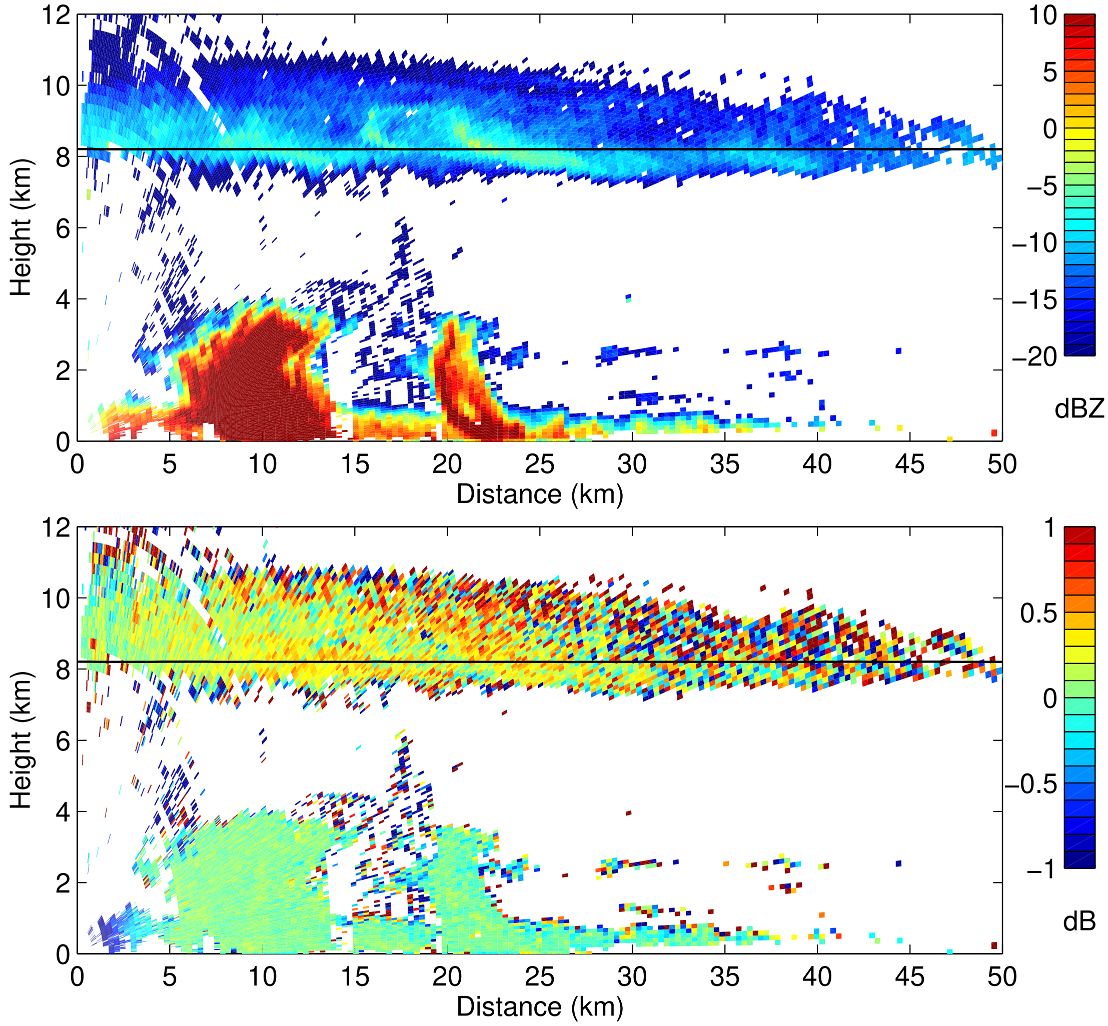

Figure 4.10: Range-height scan of 3 GHz reflectivity (top) and differential reflectivity (bottom) for Run 6.2. The scan rate of the radar was reduced to try to best follow the aircraft, the path of which is shown by the horizontal lines.

peaked at around -5 dBZ, and it can also be seen that the differential reflectivity, although noisy, is positive and varies between 0 and 0.5 dB. This indicates the presence of horizontally aligned crystals and is in contrast to the light rain beneath where the drops are predominantly spherical and Z_{DR} is very close to 0 dB.

4.4.2 Comparison of reflectivity

The slower-than-normal scan rate justified averaging over four pulses, resulting in a modest increase in accuracy and sensitivity. Then radar-measured Z and Z_{DR} were interpolated on to a line corresponding to the path of the aircraft. Figure 4.11 shows comparisons of radar-measured reflectivity (in red) and those calculated from aircraft size spectra (in black) for each run. The plots

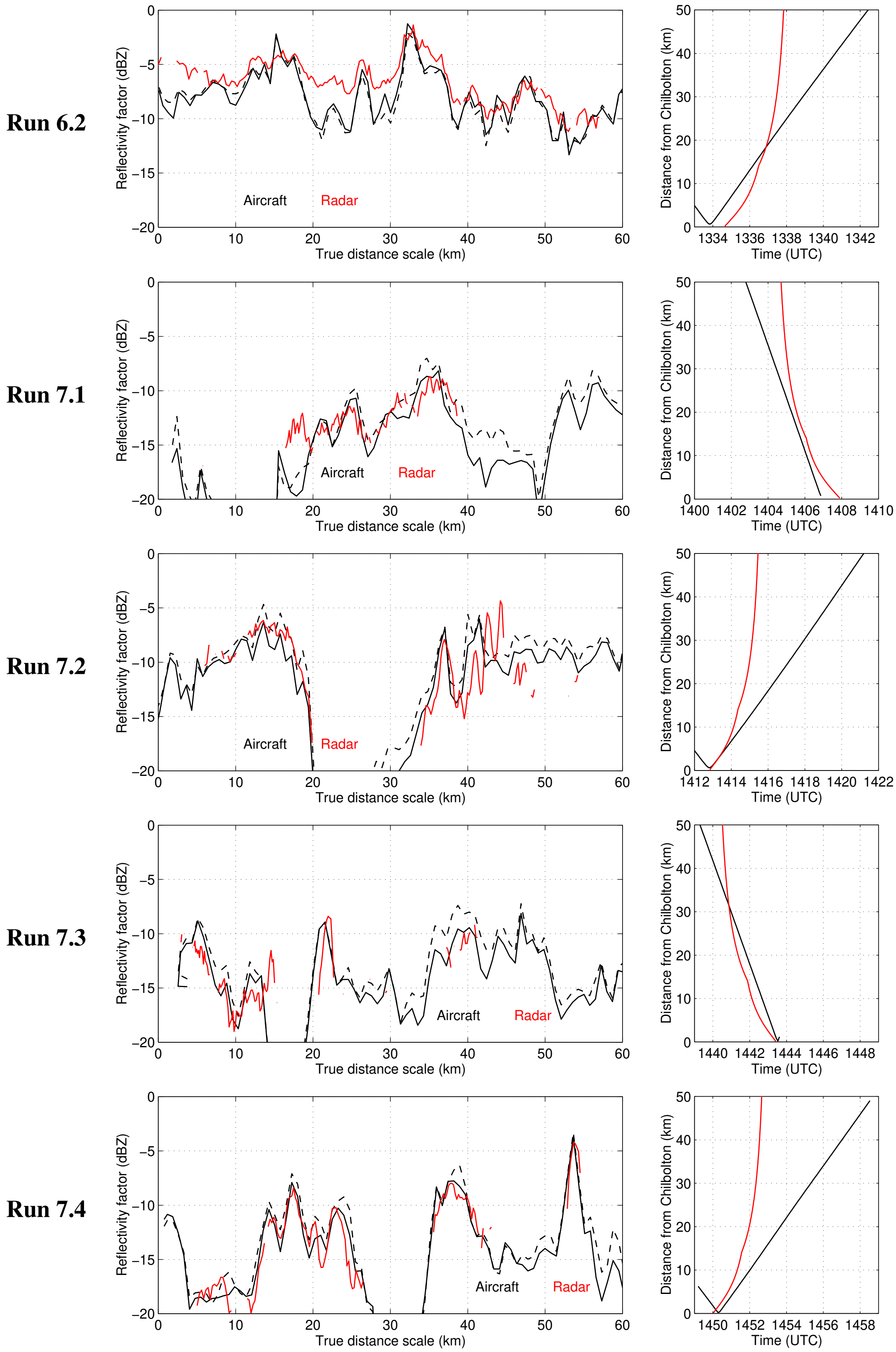

Figure 4.11: Comparison of the reflectivity measured by the radar (red lines) and that calculated from the aircraft using spectra binned by area (solid black lines) and by D_{m} (dashed black lines). The plots to the right show the corresponding distance from Chilbolton versus time for the radar beam and the aircraft.

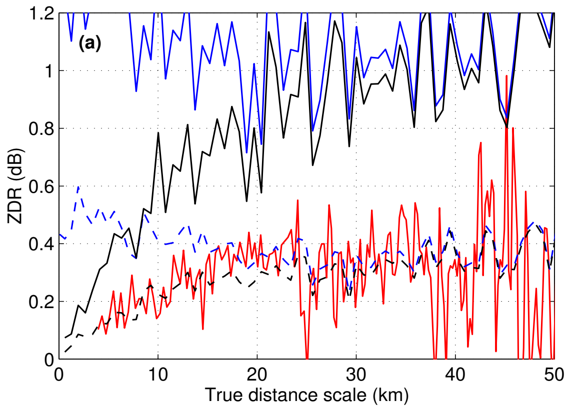

Figure 4.16: Comparison of the differential reflectivity Z_{DR} measured by radar (red lines) and calculated from aircraft size spectra binned by area (solid blue or black lines) and D_m (dashed blue or black lines). The blue lines indicate the Z_{DR} that would be measured by a horizontally-pointing radar, and the black lines show Z_{DR} calculated to take account of the elevation of the radar; it is therefore these which should be compared with the radar. Plot (a) shows the case for all crystals aligned in the horizontal, and plot (b) is for a canting angle of 33°.

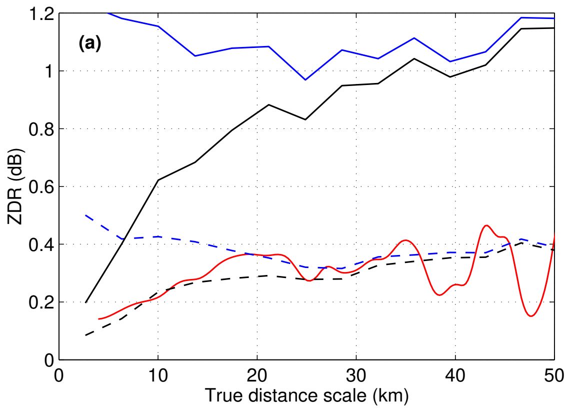

Figure 4.17: As for Fig. 4.16 but with the aircraft spectra averaged over 25 rather than 5 seconds, and the radar-measured Z_{DR} smoothed by multiple passes of a simple moving-average filter.

standard deviation of between 0.05 and 0.1 dB (Sachidananda and Zrnić 1985). At lower signal-to-noise ratios this fluctuation increases. Note that near zenith the 3 GHz radar at Chilbolton suffers greatly from ground clutter and so here the data have been rejected. Figure 4.17 shows the same as Fig. 4.16 but with the aircraft spectra averaged over 25 seconds, and the radar-measured Z_{DR} smoothed by multiple passes of a simple moving-average filter. In the first 35 km the fluctuation of the raw data is modest enough that some confidence can be ascribed to the smoothed Z_{DR}, but further out the low signal-to-noise ratio makes the raw signal much noisier.

The aircraft-calculated Z_{DR} in the plots labelled (a) in Figs. 4.16 and 4.17 were calculated assuming all crystals to be aligned horizontally. Unlike for Z, the two density functions produce distinctly different values for Z_{DR} and it appears that the lower density function gives much better

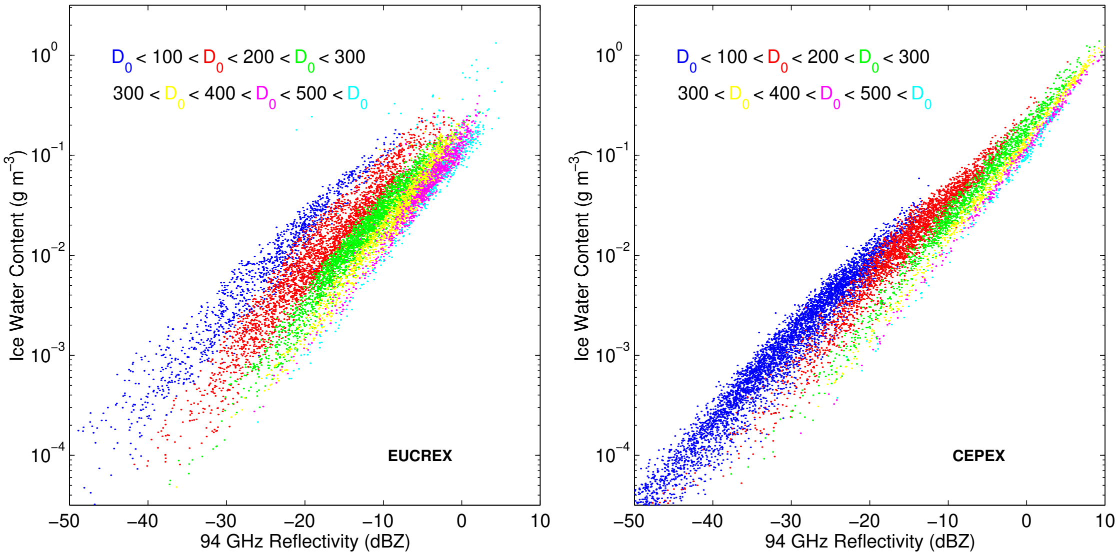

Figure 5.1: Scatterplots of ice water content versus 94 GHz reflectivity factor calculated from the EUCREX (mid-latitude) and CEPEX (tropical) aircraft datasets. The various colours represent different ranges of median volume diameter D_0 (in microns).

aircraft data from FIRE (the First ISCCP Regional Experiment), although from broadly comparable results they concluded that without size available, any estimate of IWC would be too inaccurate to be of any use for models, and also that a significant fraction of radiatively important clouds would be missed with a minimum sensitivity of -30 dBZ.

The data used by Brown et al. (1995) is shown in Fig. 5.1 as ice water content versus 94 GHz reflectivity factor, with the different colours indicating different ranges of median volume diameter. It is clear that the measurement of crystal size in addition to reflectivity would enable ice water content to be retrieved much more accurately.

The important question of how additional instruments aboard the satellite could be used to derive size has yet to be fully addressed. It was demonstrated by Intrieri et al. (1993) that crystal size can be retrieved using ground-based radar and infrared lidar due to the very different diameter-dependence of the backscattered power. They used a CO_2 lidar (10.6 µm), but gas lidars tend to be large instruments and generally unsuited to use from space. In theory a visible lidar should be able to serve the same purpose, but this has yet to be demonstrated from the ground. Additionally, reliable techniques to correct for the strong multiple scattering and attenuation at lidar wavelengths need to be developed before size measurement from space using this method could expect any success.

One possible alternative is to use two radars of different frequencies, with the higher frequency scattering sufficiently outside the Rayleigh regime that as crystal size increases, reflectiv-

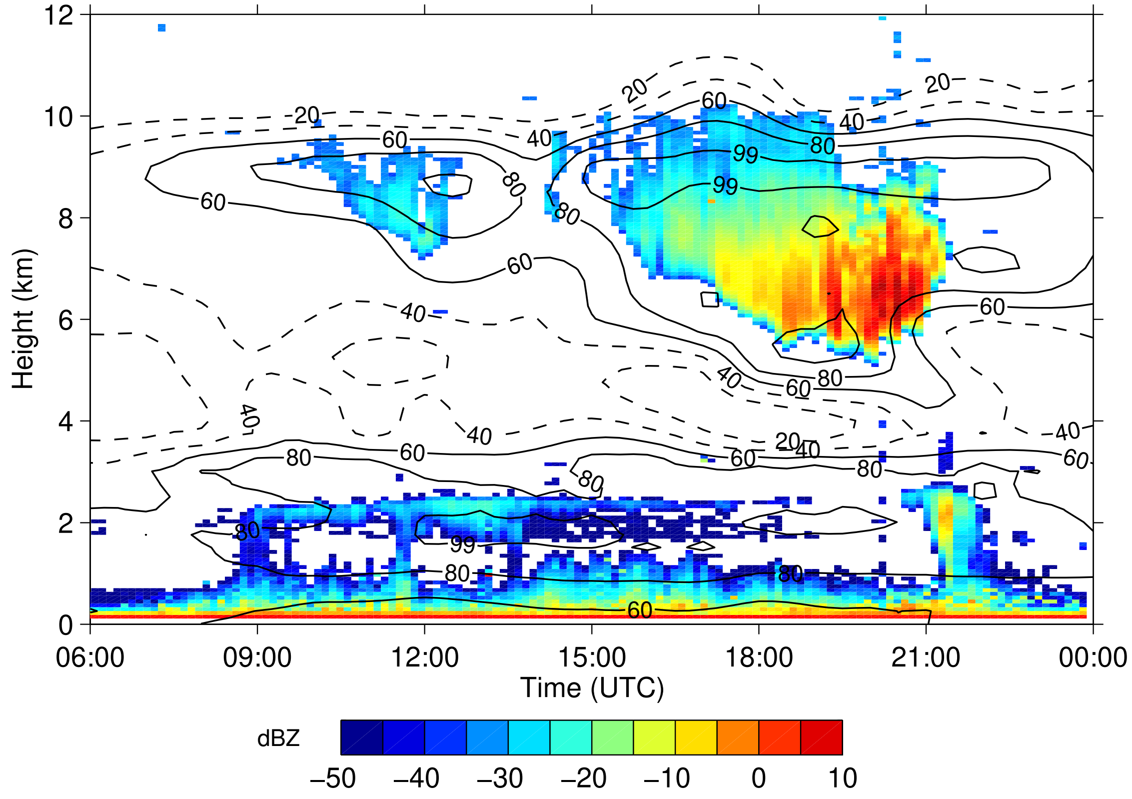

Figure 6.6: 35 GHz reflectivity factor with UKMO Unified Model relative humidity contours (%) superimposed, for part of 22 June 1996.

have attenuated the 94 GHz signal somewhat, but this could not have affected the results because of the way this radar is calibrated. A vertically-pointing lidar ceilometer was also in operation on this day but it was found that throughout the period the cirrus was overhead, the lidar signal was completely blocked by the low-level cloud; cloud base was measured as 2.1 km, and the signal was lost by 2.3 km.

Figure 6.6 shows a time series of relative humidity from the three-hourly analyses and the T+1 and T+2 forecasts of the model, superimposed on 35 GHz reflectivity factor. Model parameters over Chilbolton were calculated simply by interpolating linearly between the four nearest model gridpoints at each model level, and relative humidity was taken to be with respect to ice for temperatures below 0°C. The model has a horizontal resolution of around 17 km and at cirrus altitudes a vertical resolution of around 1 km. The raw radar data were recorded as 10 second averages with a range-gate spacing of 75 m, but in Fig. 6.6 were averaged over 8 minutes and 150 metres, enabling a 9.9 dB increase in sensitivity. There is broad agreement between the location of the cloud as indicated by the radar, and the most humid areas of the model. The sharp observed cirrus cloud base

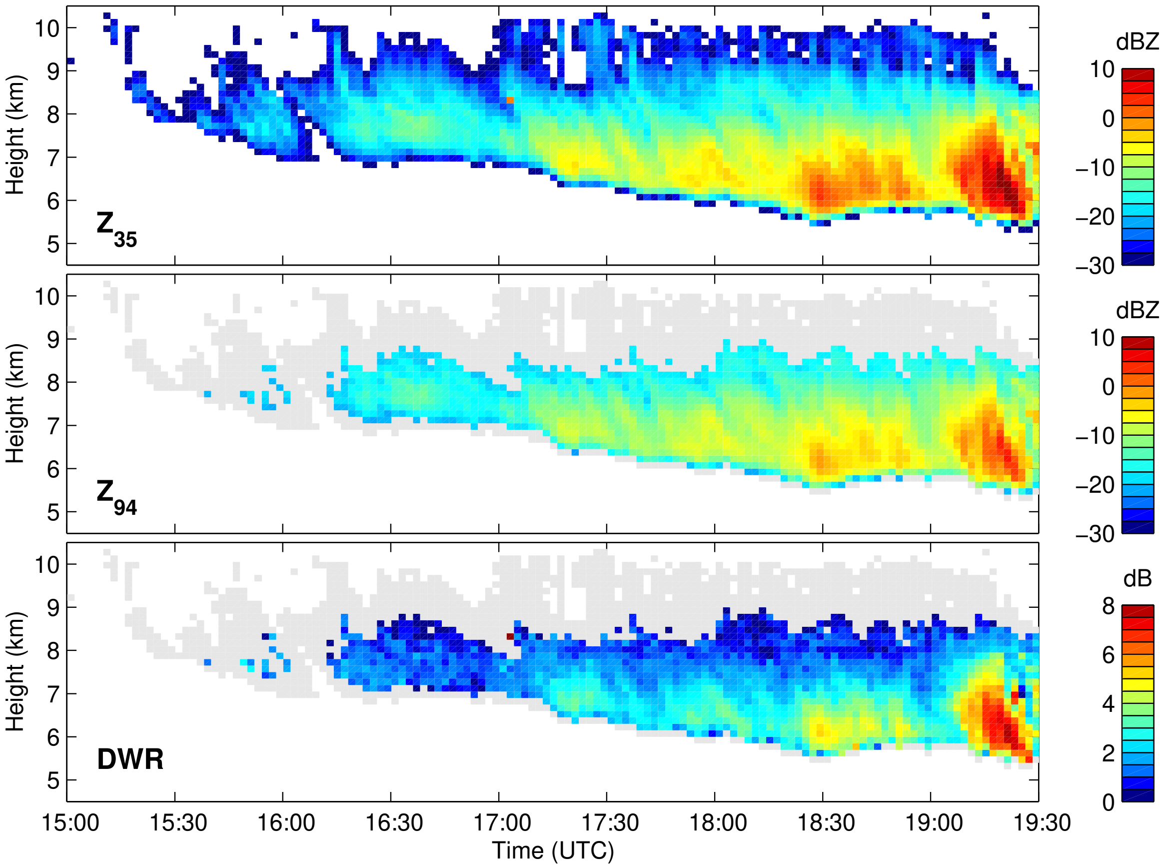

Figure 6.7: Time-series of dual-wavelength radar data obtained on 22 June 1996: (from top) 35 GHz reflectivity factor; 94 GHz reflectivity factor; dual-wavelength ratio. The light grey shading indicates where the 35 GHz radar has detected cloud but the 94 GHz has not.

can be explained by evaporation in the very dry layer beneath the cloud, although the model appears to have positioned both around a kilometre too low. Note that both insects and ground-clutter are apparent in the radar data below 1 km.

Figure 6.7 shows dual-wavelength measurements for a shorter period of the day. This time the data have been averaged over 2 minutes and 150 m. The first thing to note is that the sensitivity of the 94 GHz radar is around 10 dB lower than that at 35 GHz, and its minimum detectable reflectivity for this averaging time is only around -20 dBZ at 10 km. This is believed to be due to a technical fault which will hopefully be cured when the instrument is Dopplerised, but unfortunately in this case study it limits the application of the technique to the lower half of the cloud, and reduces the accuracy achievable. Dual-wavelength ratio is observed to rise to 7.5 dB near the bottom of the most reflective fall streak, indicating the presence of the largest crystals.

Size measurements are not possible in the upper parts of the cloud where DWR is only slightly greater than 0 dB. To determine how low DWR can get before sizing is impossible, we

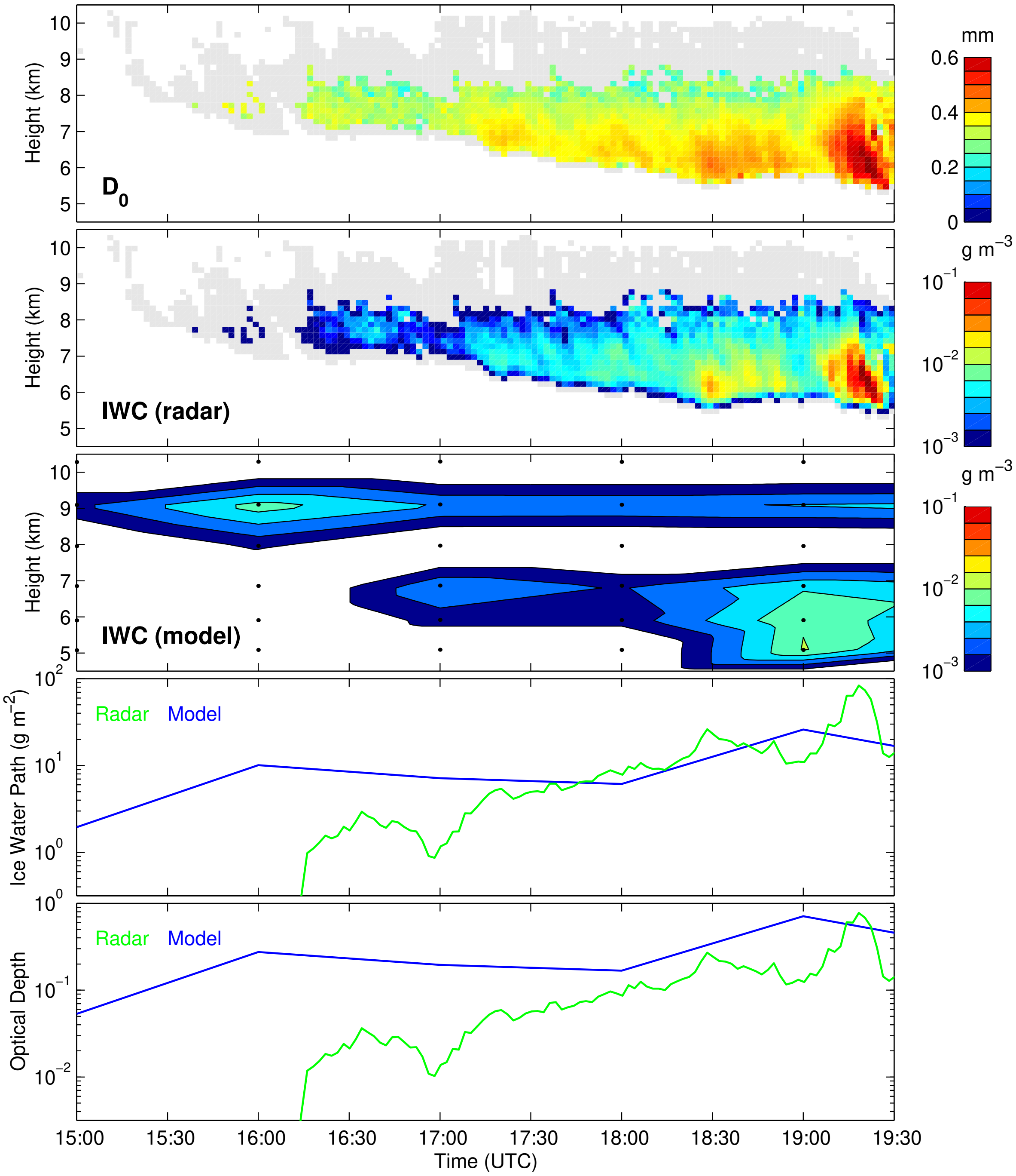

Figure 6.10: Time-series of parameters derived from the dual-wavelength radar data in Fig. 6.7: (from top) median volume diameter; ice water content derived from radar; ice water content diagnosed by the UKMO Unified Model (where the black dots indicate the model gridpoints); ice water path from the model and the radar; optical depth from the model and the radar.

tion of $r_e = 30\,\mu$m). The fact that radar-derived IWP and optical depth were only calculated from the lower half of the cloud (where sizing was possible) should not bias the results that much because the contribution from the upper half of the cloud is likely to be around an order of magnitude

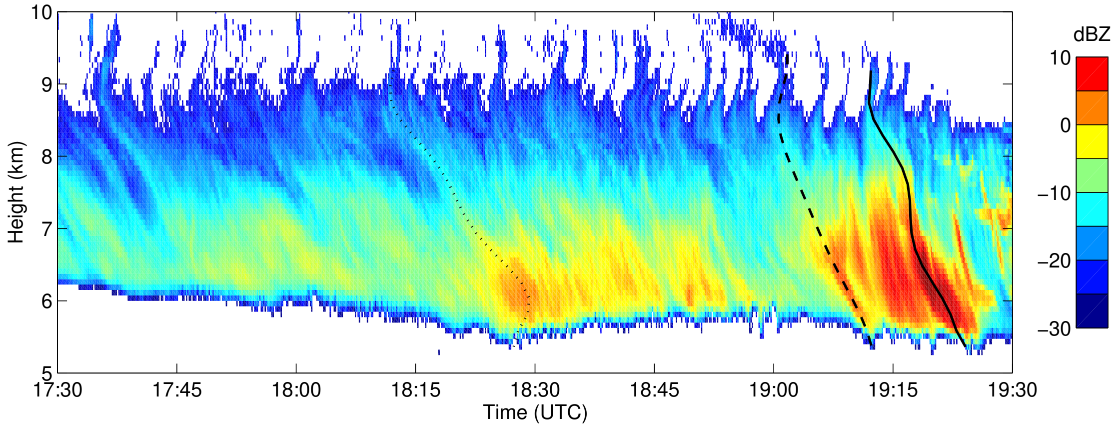

Figure 6.11: High resolution 35 GHz reflectivity factor with objectively-derived fallstreaks overlayed.

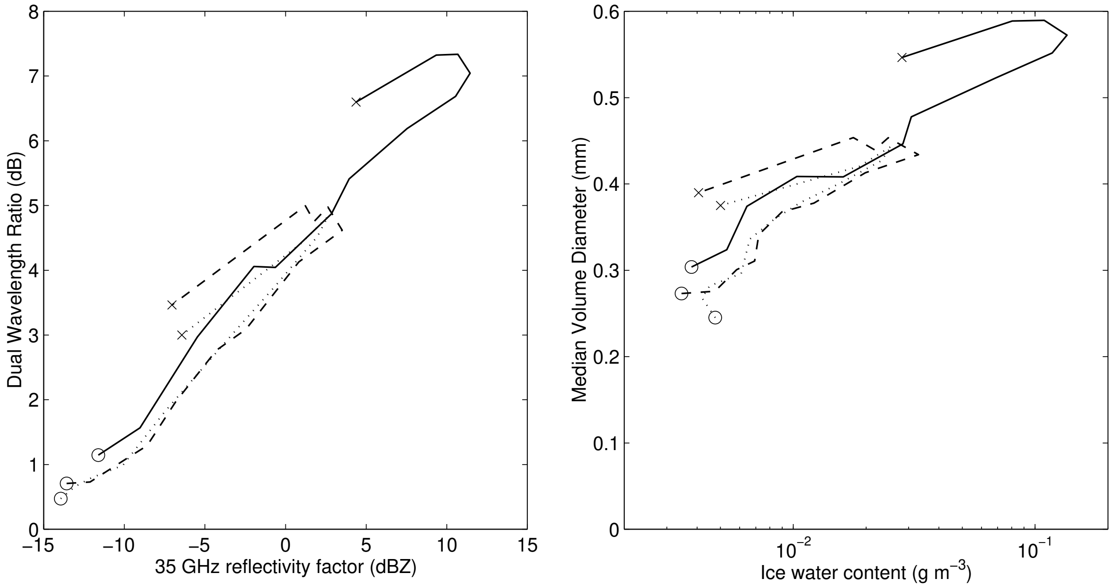

Figure 6.12: DWR against Z_{35}, and D_0 against IWC for the three fallstreaks highlighted in Fig. 6.11, using the same line-styles. The circles indicate the top of the streaks and the crosses indicate the bottom.

expressions given by (6.3) and (6.4) produce retrieved values for IWC which differ by around a factor of two. The evidence presented in Chapter 4 was in favour of the second of the two functions being correct, so that is the one we used for interpreting the observations. More work is required to confirm this conclusion if one is to have confidence in the accuracy of any radar retrieval algorithm in cirrus. It was also demonstrated that monomodal distributions such as a gamma distribution can be poor for representing crystal size distributions if radar reflectivity is to be calculated, as they tend to underestimate the number concentration of the very large crystals.

Dual-wavelength observations of a real cirrus cloud measured median volume diameters of up to 0.6 mm, and a distinct difference in the crystal size at the base and top of the cloud for a